The dopamine transporter counter-transports potassium to increase the uptake of dopamine

Claus Loland (cllo@sund.ku.dk)
University of Copenhagen https://orcid.org/0000-0002-1773-1446
Solveig Schmidt
University of Copenhagen
Mette Malle
University of Copenhagen
Anne Nielsen
University of Copenhagen
Søren Bohr
University of Copenhagen
Ciara Pugh
University of Copenhagen
Jeppe Nielsen
University of Copenhagen
Ida Poulsen
University of Copenhagen
Kasper Rand
University of Copenhagen https://orcid.org/0000-0002-6337-5489
Nikos Hatzakis
University of Copenhagen

Biological Sciences - Article

Keywords: dopamine transporter, neurotransmission, neurotransmitter: sodium symporter

Posted Date: November 3rd, 2021

DOI: https://doi.org/10.21203/rs.3.rs-1043992/v1

Version of Record: A version of this preprint was published at Nature Communications on May 4th, 2022. See the published version at https://doi.org/10.1038/s41467-022-30154-5.

Abstract

The dopamine transporter (DAT) facilitates dopamine reuptake from the extracellular space, and thereby terminates neurotransmission and refills cellular stores of dopamine. DAT belongs to the neurotransmitter:sodium symporter (NSS) family, which includes similar transporters for serotonin, norepinephrine, and GABA. A hallmark of NSS proteins is their ability to utilize the energy stored in the inward-directed Na+ gradient to drive the uphill transport of substrate. Decades ago, it was shown that the serotonin transporter also counter-transports K+, but investigations of K+-coupled transport in other NSSs have been inconclusive. Here, we show that the Drosophila dopamine transporter (dDAT) counter-transports K+. We found that ligand binding to both dDAT and human DAT is inhibited by K+ and that the conformational dynamics of dDAT in K+ is highly divergent from both the apo- and Na+-bound conformations. Furthermore, we found that K+ increased dopamine uptake by purified dDAT reconstituted in liposomes, and we visualized, in real-time, Na+ and K+ fluxes in single proteoliposomes using fluorescent ion indicators. Our results expand on the fundamentals of dopamine transport and prompt a reevaluation of the impact of K+ on other NSSs, including whether K+ counter-transport is a common mechanism for this pharmacologically important protein family.

Introduction

Dopaminergic signaling is involved in higher-order brain functions such as movement, mood, motivation, and learning[5,6]. The dopamine transporter (DAT) is responsible for the clearance of dopamine from the extracellular space and hence plays an important role in dopamine signaling intensity[6]. DAT malfunction has been associated with parkinsonism and ADHD[7,8]. In addition, DAT is the molecular target for pharmacological drugs such as methylphenidate, bupropion, and modafinil[1], and the rewarding and addictive effects of psychostimulants are linked to their interaction with the transporter[9-11]. The compounds that target DAT are classified into inhibitors and substrates but the underlying differences in mechanisms of drug action are generally poorly understood, including the reverse transport mode induced by amphetamine[12]. A prerequisite for investigating the mechanisms of action of the drugs is to understand the basal transport mechanism of the transporters.

DAT belongs to the neurotransmitter:sodium symporter (NSS) family[2], which also includes transporters of serotonin, norepinephrine, GABA, metabolites, and amino acids. It embraces species from eukaryotes, bacteria, and archaea. The NSSs share a common structural fold consisting of 12 transmembrane segments (TMs) connected by extracellular- (EL) and intracellular (IL) loops[13]. Transport is proposed to occur by a rocking-bundle mechanism, where the central binding site for substrate and ions is alternatingly accessible to either side of the membrane, caused by the movement of TM 1, 2, 6, and 7, relative to TMs 3, 4, 8, and 9[14].

It has been long known that the serotonin transporter (SERT) in addition to the symport of Na^+ possesses a counter-transport of K^+. The K^+ counter-transport is permissive and increases the k_{cat} for

serotonin[15]. This feature is thought to be unique for SERT. However, we have observed an effect of K^+ on the transport properties and conformational state of LeuT – a prokaryote NSS[16-18]. Although still controversial[19], it opens for the possibility that K^+ counter-transport might be an evolutionary preserved mechanism within the NSS family that previously have been overlooked.

K^+ shows competitive binding relative to Na^+

To address this aspect of the NSS mechanism, we turned to the *Drosophila* DAT (dDAT)[20,21]. Dopamine affinity and transport rate by dDAT is comparable to human DAT (hDAT), and the pharmacological profile of dDAT lies between that of hDAT and the human NET[22]. Using dDAT, we investigated whether K^+ is a component in dopamine transport.

The potent NET inhibitor [^{3}H]nisoxetine binds dDAT with high affinity (Extended Data Fig. 1a)[22]. If a K^+ binding site exists in dDAT with similar mechanistic features as observed for SERT[23] and LeuT[16], it should exclude substrate binding and be competitive to Na^+. To address this, we expressed full-length dDAT-8-His protein in suspension HEK293 cells (Expi293F) using the BacMam system[24,25] and purified the transporter[20]. We probed the Na^+-dependence of [^{3}H]nisoxetine binding to dDAT in mixed detergent-lipid micelles (Fig. 1a). We found that Na^+ supports the binding of 120 nM [^{3}H]nisoxetine with an EC_{50} for Na^+ of 60 [53;67] mM (mean [SEM interval]), whereas K^+ did not support [^{3}H]nisoxetine binding (Extended Data Fig. 1b). We then included various K^+ concentrations and found that K^+ dose-dependently decreased the EC_{50} value for Na^+-dependent [^{3}H]nisoxetine binding (Fig. 1a and Extended Data Table 1). A Schild plot analysis[26] of the change in EC_{50} values as a function of added K^+, estimated the affinity (K_B) for K^+ to 102 [100;105] mM (mean [SEM interval]). The slope of the linear regression in the plot was not significantly different from 1 suggesting that K^+ acts as a competitive inhibitor of Na^+ binding (Fig. 1b). We next assessed whether the inhibitory effect of K^+ is shared between dDAT and hDAT. We expressed hDAT in Expi293F cells, harvested the membranes, and measured the Na^+-dependent [^{3}H]MFZ 2-12[27] binding to hDAT in the presence and absence of K^+ (Fig. 1c). The EC_{50} value for Na^+ binding was 24 [23;26] mM (mean [SEM interval]), but increased to 121 [106;134] mM (mean [SEM interval]) by the addition of 400 mM K^+, indicating a similar inhibitory effect of K^+ in dDAT and hDAT.

K^+ induces overall stabilization of dDAT structural dynamics

If dDAT possesses a K^+ binding site with implication for function, then K^+ binding would be expected to impact the dynamics of dDAT structure. To investigate this, we probed the influence of K^+ on the overall conformational dynamics of dDAT by hydrogen-deuterium exchange MS (HDX-MS). The rate of hydrogen/deuterium exchange (HDX) of backbone amide hydrogens correlates with the specific hydrogen

bonding of higher-order protein structure[20,28]. For instance, if the binding of an ion stabilizes the region of a protein, it will typically be reflected in the HDX profile of that region. Accordingly, we probed the solution-phase HDX profile of purified dDAT in mixed micelles in 200 mM KCl. The time-dependent HDX was monitored for 85 identified dDAT peptides[20] covering ~77 % of the protein sequence (Fig. 2, Extended Data Table 2 & 3), thus providing us with a comprehensive view of the structural dynamics of the protein (Extended Data Fig. 2).

We compared the HDX data of dDAT in the presence of 200 mM K^+ relative to a control buffer of similar ionic strength where K^+ was substituted with Cs^+. We found that many regions of dDAT underwent decreased HDX in the K^+-containing buffer, which indicated widespread stabilization of dDAT structural dynamics by K^+ relative to Cs^+ (Fig. 1a, b and Extended Data Fig. 2, 3a). The stabilizing effects were localized to the core domain (TM1, 2, 6, and 7) and minor parts of TM10, 12, and the C-helix, as well as the EL1, 2, 3, 4, and IL3, 4, 5. The K^+ stabilizing effect was mainly located to regions suggested to be involved in the substrate transport process as also observed previously for Na^+ in dDAT[20]. This K^+-induced stabilization of distinct, functionally relevant regions of dDAT indicates a specific K^+ binding site in the transporter.

The comparison of the HDX profile of dDAT in Na^+- versus the K^+- state revealed that even though both ions impact the conformational dynamics in many of the same regions, the differences in HDX (ΔHDX) are of opposing magnitude for several regions (Fig. 2c, d and Extended Data Fig. 2, 3b). This argues against that K^+ simply substitutes for Na^+ and induces a Na^+-bound conformation. Relative to Na^+, K^+ induced structural stabilization of TM1b, part of the hinge region of TM1, parts of TM7, and in loop regions on the extracellular side in EL2, 3, 4 and 6. In contrast, most intracellular regions were destabilized in K^+ compared to the Na^+ state. Specifically, TM1a, TM6b, IL3, the intracellular part of TM7, and IL4 along with the intracellular parts of TM8 and TM9, showed increased dynamics in the K^+ state. Increased dynamics were also observed on the extracellular face of the transporter in EL2, part of EL3, and TM6a. The higher degree of stabilization on the extracellular face and intracellular destabilization, could suggest that K^+ induces a more inward facing dDAT state than Na^+.

dDAT transport of dopamine into proteoliposomes is increased by K^+

To explore the functional relevance of K^+ to dopamine transport, we reconstituted purified dDAT into liposomes with tight control of the intra-vesicular ionic content. The reconstituted dDAT transported [^{3}H]dopamine into the lumen of the proteoliposomes (PLs) in the presence of an inward-directed Na^+ gradient (Fig. 3a). No dopamine uptake was observed in the presence of the inhibitor nortriptyline, or when the Na^+ gradient was dissipated (Extended Data Fig. 4a).

We then compared [^{3}H]dopamine transport activity from vesicles containing intra-vesicular K^+ to vesicles containing either Cs^+ or $NMDG^+$. At all times, chloride was used as the corresponding anion. Uptake data were correlated to the total amount of active dDAT in the reconstituted system (Extended Data Fig. 4b). The inwardly directed Na^+ gradient could drive dopamine uptake regardless of the intra-vesicular cation, but the concentrative capacity decreased to about 20 % when K^+ was substituted with either Cs^+ or $NMDG^+$ (Fig. 3a and Extended Data Table 4). The transport kinetics were further investigated by [^{3}H]dopamine saturation uptake experiments (Fig. 3b). The K_m for [^{3}H]dopamine was comparable to previous observations of dDAT in intact cells[29] (Extended Data Table 5). However, we observed a significant decrease in transport velocity, when the intra-vesicular K^+ concentration was lowered from 200 mM to 150 and 100 mM, suggesting that the V_{max} of dopamine transport is dependent on intra-vesicular K^+. We also observed a drop in transport velocity when we dissipated the K^+ gradient, by having 100 mM K^+ on both sides (Fig. 3c), suggesting that the K^+ gradient contributes with a driving force for dopamine transport.

Time-resolved flux of Na^+ and K^+ mediated by dDAT

To obtain a more direct measure of dDAT mediated ionic flux, we followed in real-time, the change in intra-vesicular ion concentration in a single vesicle setup. The PLs were tethered on a surface by biotinylated lipids and visualized with ATTO-665 membrane dye using total internal reflection fluorescence microscopy (TIRFm)[30-32]. To examine the ion flux we encapsulated either a fluorescent Na^+ indicator (Sodium Green™, Tetra (Tetramethylammonium) Salt) or a fluorescent K^+ indicator (ION Potassium Green-2 TMA+ salt) in the PLs (Extended Data Figure 5a-c). The PLs were passivated on a glass surface at the bottom of a flow cell. This allowed us to measure the relative changes in ion concentrations inside individual PLs as a function of the intensity change of the fluorescence signal from the indicators (Fig. 4a). The procedure maintains the spherical morphology and structural integrity of the liposomes[30,31] and uptake of [^{3}H]dopamine was maintained (Extended Data Fig. 5d,e and 6).

We evaluated how PLs containing the Na^+ indicator responded to the application of external Na^+ and dopamine (Fig 4b). About half of the detected vesicles responded to the application of Na^+ and dopamine with an exponential increase in fluorescence intensity from the indicator followed by a plateau (Fig. 4b, c), indicating an expected increase in intra-vesicular Na^+ concentration during dopamine uptake. The number of responding vesicles decreased to about half when only Na^+ was added into the flow cell, indicating that a fraction of the PLs would take up Na^+ even in the absence of dopamine. Nortriptyline (500 µM) blocked Na^+ uptake within the timeframe of the experiment, confirming that our observations are dDAT-mediated. We did not detect passive Na^+ leakage through the lipid bilayer (Fig. 4c). After reaching the plateau, the fluorescence intensity of the Na^+ indicator decreased. We consider this an

inherent property of the indicator associated with inner filter effect (Extended Data Fig. 6e) disconnected from the Na^+ influx, and was therefore not included in the further calculations.

The measurement of DAT-mediated Na^+ flux into single PLs, lead us to proceed with the K^+-indicator to determine whether the application of Na^+ and dopamine would influence K^+ flux. To follow the intra-vesicular level of K^+, the K^+-indicator was encapsulated in PLs containing 100 mM K^+ and 100 mM $NMDG^+$. Introduction of external buffer containing dopamine, 100 mM Na^+, and 100 mM K^+ trigged an exponential decrease in the signal from the K^+-indicator, suggesting an efflux of K^+ ions (Fig. 4b). The persistent recording of K^+ flux in the absence of a K^+ gradient supports the suggestion of a K^+ counter-transport. Surprisingly, the fraction of responding liposomes was in this case not affected by dopamine. However, the response was blocked by nortriptyline, suggesting that the K^+ efflux is dDAT-mediated (Fig. 4d).

The rates of Na^+ and K^+ flux across the membrane are increased by dopamine

The time-resolved nature of the fluorescence change in the single-vesicle setup allowed us to investigate the Na^+ and K^+ flux rates in individual active PLs. We first evaluated how Na^+ transport rates were affected by dopamine and K^+. In vesicles reconstituted with $NMDG^+$, dopamine did not significantly affect the Na^+ influx rate (Fig. 4e). In contrast, in vesicles containing K^+, the addition of dopamine significantly increased the Na^+ influx rate (Fig. 4f). When comparing the dopamine-dependent Na^+ influx rates between vesicles with $NMDG^+$ and with K^+, we found that the Na^+ influx rates were increased markedly by K^+ (Fig. 4g). This suggests that the Na^+ influx associated with dopamine uptake is increased by K^+. In the absence of dopamine, the rates of Na^+ flux were not different between vesicles containing either K^+ or $NMDG^+$ (Extended Data Fig. 7), suggesting that dopamine-independent Na^+ flux is unaffected by the identity of the intra-vesicular ion.

Next, we looked at the individual fluorescence traces from liposomes loaded with fluorescent K^+-indicator. In line with our observations from the Na^+-indicator, we also here observed a significant decrease in the rate of fluorescence intensity from the K^+ indicator, suggesting an increase in K^+ efflux rates in the presence of dopamine (Fig. 4h). Taken together, the results from the single vesicle setup suggest that the number of vesicles responding with a Na^+ influx is increased with dopamine. For K^+ it is rather the rate of efflux and not the number of responding vesicles that are affected by dopamine. The correlation between the increase in rates of both Na^+ transport and K^+ counter-transport in the presence of dopamine is coherent with our suggestion that the coupling of K^+ to dopamine transport increases the rate of uptake.

Discussion

We have studied the effect of K^+ on the molecular, pharmacological, and functional properties of DAT. We showed real-time ion transport by dDAT, visualized in single vesicles resolution. All assays were performed with full-length dDAT avoiding possible artifacts from mutations or chemical protein modifications, often necessary in biophysical assays. Across methods, our results are consistent with the suggestion that K^+ takes part in dDAT-mediated dopamine transport. Our Schild plot shows that K^+ binds to dDAT with an affinity of about 100 mM, which is within a physiological concentration range for resting neurons.

Our HDX-MS data revealed that K^+ induces a conformational state that is distinct from both the dDAT apo- and Na^+-state. K^+ decreases stability mainly on the intracellular face of dDAT and stabilizes several extracellular regions. The K^+ state is coherent with a mechanism in which K^+ binding promotes an inward-facing dDAT conformation allowing the release of Na^+ and substrate on the intracellular side. It is also in agreement with the proposed K^+ states of both SERT[33] and LeuT[17] as observed using HDX-MS. Functionally, intra-vesicular K^+ causes an increase in the uptake capacity and uptake rate of dopamine relative to vesicles containing intra-vesicular Cs^+ or $NMDG^+$, and this increase is unrelated to the level of active transporters in the vesicles. This suggests that the function of K^+ is to decrease the rate-limiting step in the dDAT transport cycle or to inhibit the rebinding of Na^+ and dopamine, which otherwise can obstruct the progression of the transport cycle or even promote reverse transport. The latter has been suggested as the role for K^+ in LeuT[16].

We cannot rule out that a fraction of the reconstituted dDAT is in the inside-out orientation. However, when imposing an inward-directed Na^+ gradient we promote unidirectional transport.

The reconstitution in PLs also allows the encapsulation of fluorescent sensors such as the Na^+ and K^+ indicators. We were able to visualize the movement of ions across the membrane by dDAT in the single vesicles. We saw that Na^+ and K^+ transport could be uncoupled from dopamine transport. Both hDAT and SERT have been shown to possess both uncoupled currents and leak currents not associated with transport[34,35]. The constitutive dopamine-independent flux of Na^+ and K^+ could be parallel to the leak currents measured by electrophysiology[35]. When dopamine was added externally, it increased the rate by which K^+ was counter-transported. When both dopamine and K^+ was present on the external and intra-vesicular side respectively, the rate of Na^+ fluorescence increased, and correlated with a decrease in K^+ fluorescence. The observation is coherent with a transport-mechanism where Na^+ and dopamine uptake became coupled with K^+ counter-transport.

Our results suggest that K^+ counter-transport is a significant component of the dopamine reuptake mechanism of dDAT. It is permissive but not obligate for dopamine transport. The effects observed here align with observations on SERT[4] and LeuT[16,17], linking our results to both an evolutionary close - and a distantly related NSS, respectively. The pharmacological data presented on hDAT opens the possibility that K^+ also here could have a similar effect. Taken together, this suggests that K^+ counter-transport is

more common among the NSS family of transporters than previously anticipated and could be a rule rather than the exemption. In the broader perspective, understanding the NSS transport mechanism in molecular detail forms part of the basis for guiding the development of drugs that modulate the transporters. Furthermore, it could be important for precision medicine by allowing prediction of the functional implications of transporter single nucleotide polymorphism in individuals suffering from neuropsychiatric disorders[7,36] and thus guide the choice of drugs for treatment.

Declarations

DATA AVAILABILITY

Data supporting the findings described of this study are available from the corresponding author upon request.

ACKNOWLEDGEMENTS

We would like to thank Lone Rosenquist for technical assistance. The work was supported in part by The Independent Research Fund Denmark (7016-00272A to C.J.L.), The Lundbeck Foundation (R344-2020-1020 to C.J.L.), The Novo Nordic Foundation (NNF19OC0058496 to C.J.L.) and The Carlsberg Foundation (CF20-0345 to C.J.L.).

AUTHOR CONTRIBUTIONS

C.J.L. conceptualized the idea. S.G.S., M.G.M. and A.K.N. designed the experiments together with K.D.R., N.S.H. and C.J.L. S.G.S., M.G.M., A.K.N., S.S-R.B., C.F.P., J.C.N. and I.H.P. performed the experiments and data analysis. All authors were involved in data interpretation. S.G.S. and C.J.L. prepared the manuscript with significant contribution from all authors.

COMPETING INTERESTS

The authors declare no competing interests.

ADDITIONAL INFORMATION

Supplementary Information is available for this paper.

Correspondence and requests for materials should be addressed to CJL.

References

1 Aggarwal, S. & Mortensen, O. V. Overview of Monoamine Transporters. *Curr Protoc Pharmacol* **79**, 12.16.11-12.16.17, doi:10.1002/cpph.32 (2017).

2 Saier, M. H., Jr., Tran, C. V. & Barabote, R. D. TCDB: the Transporter Classification Database for membrane transport protein analyses and information. *Nucleic Acids Res* **34**, D181-D186 (2006).

3 Bröer, S. & Gether, U. The solute carrier 6 family of transporters. *Br J Pharmacol* **167**, 256-278, doi:10.1111/j.1476-5381.2012.01975.x (2012).

4 Rudnick, G. & Nelson, P. J. Platelet 5-hydroxytryptamine transport, an electroneutral mechanism coupled to potassium. *Biochemistry* **17**, 4739-4742, doi:10.1021/bi00615a021 (1978).

5 Wise, R. A. Dopamine, learning and motivation. *Nat Rev Neurosci* **5**, 483-494, doi:10.1038/nrn1406 (2004).

6 Sotnikova, T. D., Beaulieu, J. M., Gainetdinov, R. R. & Caron, M. G. Molecular biology, pharmacology and functional role of the plasma membrane dopamine transporter. *CNS. Neurol. Disord. Drug Targets* **5**, 45-56 (2006).

7 Hansen, F. H. *et al.* Missense dopamine transporter mutations associate with adult parkinsonism and ADHD. *J Clin Invest* **124**, 3107-3120, doi:10.1172/JCI73778 (2014).

8 Cook, E. H., Jr. *et al.* Association of attention-deficit disorder and the dopamine transporter gene. *Am J Hum Genet* **56**, 993-998 (1995).

9 Beuming, T. *et al.* The binding sites for cocaine and dopamine in the dopamine transporter overlap. *Nat Neurosci* **11**, 780-789, doi:10.1038/nn.2146 (2008).

10 Giros, B., Jaber, M., Jones, S. R., Wightman, R. M. & Caron, M. G. Hyperlocomotion and indifference to cocaine and amphetamine in mice lacking the dopamine transporter. *Nature* **379**, 606-612 (1996).

11 Chen, R. *et al.* Abolished cocaine reward in mice with a cocaine-insensitive dopamine transporter. *Proc. Natl. Acad. Sci. U. S. A* **103**, 9333-9338 (2006).

12 Robertson, S. D., Matthies, H. J. G. & Galli, A. A closer look at amphetamine-induced reverse transport and trafficking of the dopamine and norepinephrine transporters. *Mol Neurobiol* **39**, 73-80, doi:10.1007/s12035-009-8053-4 (2009).

13 Yamashita, A., Singh, S. K., Kawate, T., Jin, Y. & Gouaux, E. Crystal structure of a bacterial homologue of Na+/Cl–dependent neurotransmitter transporters. *Nature* **437**, 215-223 (2005).

14 Forrest, L. R. & Rudnick, G. The rocking bundle: a mechanism for ion-coupled solute flux by symmetrical transporters. *Physiology. (Bethesda.)* **24**, 377-386, doi:24/6/377

[pii];10.1152/physiol.00030.2009 [doi] (2009).

15 Keyes, S. R. & Rudnick, G. Coupling of transmembrane proton gradients to platelet serotonin transport. *J Biol Chem* **257**, 1172-1176 (1982).

16 Billesbølle, C. B. *et al.* Transition metal ion FRET uncovers K+ regulation of a neurotransmitter/sodium symporter. *Nature Communications* **7**, 12755, doi:10.1038/ncomms12755 (2016).

17 Merkle, P. S. *et al.* Substrate-modulated unwinding of transmembrane helices in the NSS transporter LeuT. *Sci Adv* **4**, eaar6179, doi:10.1126/sciadv.aar6179 (2018).

18 Khelashvili, G. *et al.* Conformational Dynamics on the Extracellular Side of LeuT Controlled by Na+ and K+ Ions and the Protonation State of Glu290. *J Biol Chem* **291**, 19786-19799, doi:10.1074/jbc.M116.731455 (2016).

19 Zhang, Y. W. *et al.* Structural elements required for coupling ion and substrate transport in the neurotransmitter transporter homolog LeuT. *Proc Natl Acad Sci U S A* **115**, E8854-e8862, doi:10.1073/pnas.1716870115 (2018).

20 Nielsen, A. K. *et al.* Substrate-induced conformational dynamics of the dopamine transporter. *Nat Commun* **10**, 2714, doi:10.1038/s41467-019-10449-w (2019).

21 Penmatsa, A., Wang, K. H. & Gouaux, E. X-ray structure of dopamine transporter elucidates antidepressant mechanism. *Nature* **503**, 85-90, doi:nature12533 [pii];10.1038/nature12533 [doi] (2013).

22 Pörzgen, P., Park, S. K., Hirsh, J., Sonders, M. S. & Amara, S. G. The antidepressant-sensitive dopamine transporter in Drosophila melanogaster: a primordial carrier for catecholamines. *Mol Pharmacol* **59**, 83-95, doi:10.1124/mol.59.1.83 (2001).

23 Humphreys, C. J., Beidler, D. & Rudnick, G. Substrate and inhibitor binding and translocation by the platelet plasma membrane serotonin transporter. *Biochem Soc Trans* **19**, 95-98, doi:10.1042/bst0190095 (1991).

24 Dukkipati, A., Park, H. H., Waghray, D., Fischer, S. & Garcia, K. C. BacMam system for high-level expression of recombinant soluble and membrane glycoproteins for structural studies. *Protein Expr. Purif* **62**, 160-170, doi:S1046-5928(08)00213-1 [pii];10.1016/j.pep.2008.08.004 [doi] (2008).

25 Goehring, A. *et al.* Screening and large-scale expression of membrane proteins in mammalian cells for structural studies. *Nat. Protocols* **9**, 2574-2585 (2014).

26 Wyllie, D. J. & Chen, P. E. Taking the time to study competitive antagonism. *Br J Pharmacol* **150**, 541-551, doi:10.1038/sj.bjp.0706997 (2007).

27 Newman, A. H., Zou, M. F., Ferrer, J. V. & Javitch, J. A. [3H]MFZ 2-12: a novel radioligand for the dopamine transporter. *Bioorg Med Chem Lett* **11**, 1659-1661, doi:10.1016/s0960-894x(01)00271-2 (2001).

28 Skinner, J. J., Lim, W. K., Bédard, S., Black, B. E. & Englander, S. W. Protein dynamics viewed by hydrogen exchange. *Protein Sci* **21**, 996-1005, doi:10.1002/pro.2081 (2012).

29 Wang, K. H., Penmatsa, A. & Gouaux, E. Neurotransmitter and psychostimulant recognition by the dopamine transporter. *Nature* **521**, 322-327, doi:10.1038/nature14431 (2015).

30 Thomsen, R. P. *et al.* A large size-selective DNA nanopore with sensing applications. *Nat Commun* **10**, 5655, doi:10.1038/s41467-019-13284-1 (2019).

31 Bohr, S. S., Thorlaksen, C., Kuhnel, R. M., Gunther-Pomorski, T. & Hatzakis, N. S. Label-Free Fluorescence Quantification of Hydrolytic Enzyme Activity on Native Substrates Reveals How Lipase Function Depends on Membrane Curvature. *Langmuir* **36**, 6473-6481, doi:10.1021/acs.langmuir.0c00787 (2020).

32 Hatzakis, N. S. *et al.* How curved membranes recruit amphipathic helices and protein anchoring motifs. *Nat Chem Biol* **5**, 835-841, doi:10.1038/nchembio.213 (2009).

33 Möller, I. R. *et al.* Conformational dynamics of the human serotonin transporter during substrate and drug binding. *Nat Commun* **10**, 1687, doi:10.1038/s41467-019-09675-z (2019).

34 Mager, S. *et al.* Conducting states of a mammalian serotonin transporter. *Neuron* **12**, 845-859 (1994).

35 Sonders, M. S., Zhu, S. J., Zahniser, N. R., Kavanaugh, M. P. & Amara, S. G. Multiple ionic conductances of the human dopamine transporter: the actions of dopamine and psychostimulants. *J Neurosci* **17**, 960-974 (1997).

36 Herborg, F., Andreassen, T. F., Berlin, F., Loland, C. J. & Gether, U. Neuropsychiatric disease-associated genetic variants of the dopamine transporter display heterogeneous molecular phenotypes. *Journal of Biological Chemistry* **293**, 7250-7262, doi:10.1074/jbc.RA118.001753 (2018).

37 Masson, G. R. *et al.* Recommendations for performing, interpreting and reporting hydrogen deuterium exchange mass spectrometry (HDX-MS) experiments. *Nat Methods* **16**, 595-602, doi:10.1038/s41592-019-0459-y (2019).

Methods

Protein expression and purification. Full-length dDAT was produced using baculovirus-mediated transduction of Expi293F suspension cells and purified as previously described[20]. Briefly, membranes

were prepared by sonication, homogenized and solubilized in buffer containing 20 mM Tris, pH 8.0, 150 mM NaCl, 20 mM *n*-dodecyl β-D-maltoside (DDM), 4 mM cholesteryl hemisuccinate (CHS), 5 µg/ml benzamidine, and 10 µg/ml leupeptin. Detergent-solubilized dDAT was incubated with nickel-charged metal affinity resin, and washed in buffer containing 40 mM Tris, pH 8.0, 300 mM NaCl, 5% glycerol, 14 µM lipids (POPC, POPE, and POPG at a weight ratio of 3:1:1), 1 mM DDM, 0.2 mM CHS supplemented with 5 µg/ml benzamidine and 10 µg/ml leupeptin with a gradient of imidazole. The protein was eluted from the affinity column with buffer supplemented with 300 mM imidazole. The protein was spin-concentrated and loaded on a FLPC size exclusion column to increase purity and remove imidazole from the buffer. Finally, the protein was spin-concentrated and stored at -80°C for further use. All procedures were performed on ice or at 4°C.

Full-length hDAT was expressed using the same approach as for dDAT. The cells were harvested, and membranes were prepared by sonication in buffer containing 30 mM NaHEPES pH 8.0, 30 mM NaCl, 5 mM KCl, 5 mM Ethylenediaminetetraacetic acid (EDTA), 7 mM $MgCl_2$, 10% (w/v) sucrose, 5 µg/ml benzamidine, 10 µg/ml leupeptin, PI, 2 µg/ml DNase I, and 2 µg/ml RNase A. The membranes were pelleted by ultracentrifugation and washed in buffer containing 30 mM NaHEPES pH 8.0, 1 M NaCl, 5 µg/ml benzamidine, 10 µg/ml leupeptin, PI and 10 mM DTT by homogenization. This step was repeated twice. The membranes were homogenized in a 30 mM NaHEPES pH 8.0, 30 mM NaCl, 5 mM KCl, 10% (w/v) sucrose and 10 mM DTT buffer and stored at -80°C. All steps were performed on ice or at 4°C.

[^{3}H]Nisoxetine binding. Na^+-dependence of [^{3}H]nisoxetine binding to dDAT was determined using 0.5 mg ml^{-1} of dDAT WT mixed with 12 nM [^{3}H]nisoxetine (Perkin Elmer, 80.4 Ci $mmol^{-1}$), 108 nM nisoxetine, and dDAT storage buffer (20 mM Tris-HCl (pH 8.0), 0.05% (w/v) DDM, 0.01% (w/v) CHS, 14 mM lipids (3:1:1, POPC:POPE:POPG)) supplemented with the indicated NaCl and KCl concentrations. The ionic strength was maintained by substituting Na^+ and K^+ with $NMDG^+$. The indicated conditions were added to a clear-bottom, 96-well plate (Corning) and incubated with agitation at 4°C. 5% (v/v) YSi-Cu His-Tag SPA beads (Perkin Elmer) was added to each well. Plates were sealed, mixed at RT on an agitator and left to settle at RT for 2h. Plates were counted on a 2450 MicroBeta^2 microplate counter (PerkinElmer).

[^{3}H]MFZ 2-12 binding. Na^+-dependence of [^{3}H]MFZ 2-12 binding to hDAT was determined using 400 µg (wet-weight) of membranes mixed with 30 nM [^{3}H]MFZ 2-12 (specific activity 30 Ci/mM) in a 10 mM NH_4PO_4 pH 8.0 buffer supplied with the indicated NaCl and KCl concentrations. The ionic strength was maintained by substituting Na^+ and K^+ with $NMDG^+$. The indicated conditions were added to a clear, round-bottom, 96-well plate (Corning) and mixed briefly at RT on an agitator. The plate was sonicated for 30 seconds in a bath sonicator and incubated for 90 min at RT on an agitator. To determine [^{3}H]MFZ 2-12

binding to hDAT, the 96-well plate was placed on a cell harvester (Tomtec harvester 96 match II) and the membranes were trapped on a 96 well glass fiber filter (Filtermat B – GF/B, Perkin Elmer) soaked in 1.5% poly(ethyleneimine) solution. The glass fiber filter was washed with 1 liter ice-cold buffer containing 10 mM NH_4PO_4 pH 8.0 and 1 M NaCl. Hereafter, the filter was dried and MeltiLex B/HS (Perkin Elmer) was melted onto the filter. The filter was counted in a 2450 MicroBeta2 microplate counter (PerkinElmer). Non-specific binding was determined by addition of 2 µM nomifensine.

Data analysis of radiolabelled substrate binding. Na^+-dependence of radioligand binding to dDAT and hDAT data in varying K^+ conditions were fitted as a non-linear regression (curve fit) through a sigmoidal dose-response (variable slope) equation, otherwise known as a four-parameter logistic equation (Prism 8, GraphPad Software). This fit derived potency estimates (EC_{50} values) i.e. the [Na^+] concentration (A) that displays half-maximal [^{3}H]nisoxetine or [^{3}H]MFZ 2-12 binding, according to the upper (B_{max}) and lower plateaus of the sigmoid. Data were normalized to the top and bottom plateau for each K^+ condition. For dDAT data, Schild plots were calculated using the EC_{50} values for Na^+ in the presence (A') and absence (A) of the antagonist K^+ (B), producing the dose ratios for the differing K^+ conditions (dr = A'/A). Values of log(dr-1) were plotted as a function of their corresponding log[B] values. The affinity of K^+ for dDAT (K_B) was determined using the Schild equation: $log(dr\text{-}1) = log[B]\text{-}K_B$

Hydrogen-deuterium exchange mass spectrometry. The K^+ state was induced by dialyzing affinity-purified dDAT against buffer containing 40 mM Tris, pH 8.0, 200 mM KCl, 5% glycerol, 14 µM lipids (POPC, POPE, and POPG at a weight ratio of 3:1:1), 1 mM DDM, and 0.2 mM CHS at 4°C. Dialyzed dDAT was equilibrated at a concentration of 1.5 µM at 25°C for 30 min. Deuterium exchange was initiated by diluting the protein samples 1:4 with 94% D_2O buffer 40 mM Tris, pH 8.0, 200 mM KCl, 5% glycerol, 14 µM lipids (POPC, POPE, and POPG at a weight ratio of 3:1:1), 1 mM DDM, 0.2 mM CHS at 25°C. At defined time points (0.25 min, 1 min, 10 min, 60 min, and 480 min), the labeling reaction was quenched by mixing (1:1) aliquots of 15 pmol dDAT with ice-cold quench buffer (220 mM phosphate buffer, pH 2.3, 2 M urea). Samples were stored at -80°C until further use. All time points were performed in triplicate. The isotopic exchange was performed simultaneously with the Cs^+ and Na^+ states as described previously[20].

Prior to mass analysis, quenched samples were rapidly thawed and injected into a cooled (0°C) nanoACQUITY UPLC HDX system (Waters). Protein samples were digested online at 20°C on an in-house packed immobilized pepsin column prepared using pepsin agarose resin (Thermo Fisher scientific). The resulting peptides were rapidly desalted on a C8 trap column (VanGuard pre-column ACQUITY UPLC BEH C8 1.7 µm, Waters) for 3 min at a flow rate at 200 µl/min solvent A (0.23% formic acid in water, pH 2.5) and separated by reversed-phase chromatography over a C8 analytical column (ACQUITY UPLC BEH C8 1.7 µm, 100 nm, Waters) with a C8 trap column in front using a linear gradient from 8 – 30% solvent B (0.23% formic acid in acetonitrile) over 10 min at a flow rate of 40 µl/min. Mass analysis was conducted on a hybrid Q-TOF SYNAPT G2-Si mass spectrometer (Waters) equipped with a standard ESI source

operated in positive ion mode. Mass spectra were lock-mass corrected against Glu-fibrinopeptide B. Ion mobility separation was used to enhance peak capacity and minimize spectral overlap.

HDX-MS data for the K^+ state was acquired simultaneously with the Cs^+ and Na^+ states previously reported[20]. Maximum-labeled control samples shown here are from our previous study[20], and thus, were prepared, processed and analyzed as earlier described. Peptide identification from non-deuterated samples is also described in our previous study[20].

HDX-MS data evaluation and statistical analysis. The deuterium exchange levels were calculated for all identified peptides using DynamX 3.0 (Waters) with manual verification of all peptide assignments. Noisy and overlapping spectral data were discarded from the HDX-MS analysis. To allow for quantitative comparison of samples not measured on the same day, back-exchange was calculated and used to normalize deuterium uptake values between measuring days as previously described[20]. Also as described previously[20], the deuterium uptake of individual states were compared for all identified peptides in Microsoft Excel (Microsoft) using either a homoscedastic or a heteroscedastic Student's *t* test ($\alpha = 0.01$) depending on an F-test ($\alpha = 0.05$) that compared the variance of deuterium uptake from two different states for each single peptide at a single time point. For each peptide, a difference in HDX between two states was only considered significant if two consecutive time points showed a significant difference in deuterium uptake ($p < 0.01$). Furthermore, differences in HDX between the Cs^+ and K^+ states and the Na^+ and K^+ states had to exceed threshold values of 0.24 Da and 0.20 Da, respectively, which corresponded to the 95% confidence interval (CI) calculated according to:

$$\mathrm{CI} = \bar{x} \pm t \cdot \frac{\sigma}{\sqrt{n}}$$

Here is the average difference in deuterium content assuming a zero-centered distribution (x = 0), *t* is 4.303 for the 95% CI with 2 degrees of freedom, σ is the pooled propagated standard deviation of differences in deuterium content for all peptides across all time points (i.e. 0.25 – 480 min) for the two states compared, and n is the number of replicate samples (n = 3). HDX results were mapped onto the dDAT crystal structure (PDB ID: 4XP1) using PyMOL.

The HDX Summary Table (Extended Data Table 2) and the HDX Data Table (Extended Data Table 3) are included according to the community-based recommendations for HDX data availability[37].

Reconstitution of dDAT into liposomes. Liposomes were prepared from asolectin:cholesterol:brain polar lipid extract (Avanti) in molar ratio 60:17:20 in buffer (20 mM HEPES (pH 7.5), 200 mM KCl). The lipid mix was dried under a stream of N_2 for 2 h. The lipid film was suspended in buffer to 10 mg lipid/ml by

alternating vortexing and bath sonication. The liposomes went through five freeze-thaw cycles, and were extruded with a mini extruder(Avanti) through a polycarbonate filter with 400 nm pore size. The liposomes were diluted to 4 mg lipid/ml and mixed with purified dDAT (protein concentration in storage buffer, 2 mg/ml) in a 1:150 protein:lipid (wt/wt) ratio. After 30 min incubation under slow rotation at 7°C, SM-2 bio-beads equilibrated in buffer (20 mM HEPES (pH 7.5), 200 mM KCl) were added in a 35 mg (semi-dry)/ml beads to buffer ratio. SM-2 bio-beads were added again after 30 min, after 60 min and after 15 h. After the last addition, beads and PLs incubated for 2 h. Between additions, the sample incubated at 7°C under slow rotation. Bio-beads were removed by filtration. The proteoliposome (PL) sample was split into centrifugation tubes and diluted 25 times in the final intra-vesicular buffer (200 mM chloride salt, 20 mM HEPES (pH 7.5)) and spun at 40,000 rpm (Thermo Scientific, T-865 fixed angle rotor) for 1 h at 4°C. Subsequently, the pelleted PLs were re-suspended to 10 mg lipid/ml in their final intra-vesicular buffer, and frozen in liquid N_2 in appropriate aliquots until use. PLs for TIRFm were made as described with the following additions to the protocol. In the lipid mix 1:1000 molecular ratio of biotinylated PEG-DOPE and ATTO-655-DOPE was added. At all times, the sample was shielded from light to protect the fluorophores. After two freeze-thaw cycles the liposomes were split in two, and 10 mM Na^+-sensor (Sodium Green™, Tetra (Tetramethylammonium from ThermoFisher) Salt or K^+-sensor (ION Potassium Green-2 TMA+ Salt from Abcom) was added.

[^{3}H]Dopamine uptake experiments. PLs were thawed and extruded through a 400 nm polycarbonate filter. The uptake assay was performed in 96-well ultra-low attachment, round bottom plates at 25°C. Nonspecific binding and uptake across the lipid bilayer were measured using PLs incubated with 100 µM nortriptyline for 20 min prior to uptake. To start the uptake experiment, the PLs were diluted in freshly made uptake buffer with [^{3}H]dopamine to a final concentration of 0.5 mg lipid/ml. The total reaction volume was 200 ul. The uptake buffer (20 mM HEPES (pH 7.5), 1 mM EDTA, 1 mM L-ascorbic acid) for time-dependent uptake contained 200 mM NaCl, and for concentration-dependent uptake it contained 100 mM NaCl and 100 mM NMDG-Cl. For time-dependent uptake, 0.5 µM [^{3}H]dopamine with a specific activity of 4.54 Ci/mmol was used. For concentration-dependent uptake [^{3}H]dopamine with a specific activity of 5.14 Ci/mmol was used from [50 - 500 nM] and 1.542 Ci/mmol from [1 - 5 µM]. For concentration-dependent uptake, the reaction time was 3 min, which allowed an approximate measure of the initial rate at each substrate concentration to be obtained. To terminate the reaction, the PLs were trapped on a 96 well glass fiber filter (Filtermat B – GF/B, Perkin Elmer) pre-soaked in 1.5% poly(ethyleneimine) using a Tomtec harvester (96 match II). Each filter position was washed with 1 ml freshly made, cold wash buffer (20 mM HEPES (pH 7.5), 200 mM KCl, 1 mM EDTA, 1 mM L-ascorbic acid). Hereafter, the filter was dried and MeltiLex B/HS (Perkin Elmer) was melted onto the filter. The filter was counted in a 2450 MicroBeta^2 microplate counter (PerkinElmer).

Measuring relative amount of active transporters in proteoliposomes. From the extruded liposomes with different intra-vesicular buffers, a sample was taken from each condition and diluted 25x in dDAT storage buffer supplemented to 15 % glycerol, 1% DDM, 4 mM CHS at 7°C for 15 h to dissolve the PLs and re-suspend the protein in detergent. The detergent suspended dDAT was diluted 10x in dDAT storage buffer supplemented with 600 nM [^{3}H]nisoxetine (4.02 Ci/mmol) and 7% scintillation beads binding to dDAT via the His-tag. [^{3}H]Nisoxetine binding was measured on a 2450 MicroBeta^2 microplate counter after 30 min incubation at room temperature and again after 24 h incubation at 7°C. Non-specific binding was measured in the presences of a saturating nortriptyline concentration (200 µM) and subtracted from the c.p.m. measured in total binding. The specific maximum binding was regarded as a measure of the number of active transporters in each condition, and was used to normalize the uptake data to the amount of active transporters in the given condition.

Data analysis [^{3}H]dopamine uptake. For time-dependent dopamine uptake, the data were normalized to dDAT activity from each condition. Non-specific [^{3}H]dopamine binding measured in the presence of nortriptyline was subtracted. Normalized specific uptake data were fitted a one phase association using GraphPad Prism 7.0.

$$y(t) = p * e^{(-k*t)}$$

Where p is the maximal uptake (the amplitude) and k is the rate constant in min^{-1}, t is time in min and y is uptake in c.p.m. after normalization to transporter concentration. Subsequently, data from each experiment were normalized to the value of p from the condition with the highest maximal uptake. The normalized data sets from each experiment were combined and re-fitted to the one phase association.

For concentration dependent uptake, the data were normalized to dDAT activity from each condition. Non-specific [^{3}H]dopamine binding measured in the absence of a Na^+ gradient was subtracted. Normalized specific uptake data were fitted to the Michaelis-Menten equation. Subsequently, the data were normalized to the V_{max} value determined from the condition with the highest V_{max}. The normalized data sets from each experiment were combined and re-fitted to the Michaelis-Menten equation. [^{3}H]dopamine uptake experiments were done in triplicates and repeated minimum 3-4 times using dDAT obtained from at least 2 different purifications and reconstitutions unless otherwise stated.

TIRF Microscopy setup. All single PL experiments were acquired using an inverted total internal reflection fluorescence microscope model IX83 from Olympus. The microscope setup was equipped with an EMCCD camera model imagEM X2 from Hamamatsu and a 100x oil immersion objective model UAPON 100XOTIRF from Olympus and an emission quad band filter cube, as to block out laser light in the

emission pathway. All data were recorded using three solid state laser lines from Olympus at 488 nm, 532 nm and 640 nm in order to excite ATTO 655 membrane dye and the two ion indicators Potassium Green-2 and Sodium Green™. The data were acquired using a penetration depth at 200 nm, with a dynamic range of 16-bit grayscale and an image dimension of 512 times 512 pixels, corresponding to a physical field of view length of 81.92 µm. A peristaltic flow-pump was installed on top of the TIRF setup, as to automatically flow in both dopamine, inhibitor and uptake buffers during the real time recordings.

TIRF recordings of single proteoliposome assay. Glass surfaces were prepared using plasma cleaned glass slice with fastened sticky-Slide VI 0.4 from Ibidi and functionalized using PLL-g-PEG and PLL-g-PEG-biotin in a 100 to 1 ratio followed by a neutravidin layer [30,31]. Each glass surface contains 6 chambers that are independently utilized for liposomes immobilization and imaging. The liposomes were flowed into the selected microscope chamber using the pump setup for immobilization to obtain a liposome density of 200-250 liposomes per field of view. Unbound liposomes were washed away with 3x chamber volumes of buffer. Using CellSens imaging software from Olympus, the image recordings were fully automated. Briefly, we recorded a 6-field of view in parallel with a temporal resolution of 3.7 sec/cycle for Na^+ uptake and 3.4 sec/cycle for K^+ outflow with a total of 700 cycles per experiment corresponding to a total experimental timeframe of 43 - 40 minutes, respectively. Real-time recording was started with the same buffer in the flow cell as inside the PLs, then the buffer was exchanged using the pump for the 0.5 mL of the respective uptake buffer with a flowrate of 0.5 mL/min.

Compositions for uptake and intra-proteoliposomal buffers and substrate concentration for TIRF recording. Monitoring the outward K^+ transport, the intra-proteoliposomal buffer was composed of: 10 mM ION Potassium Green-2 TMA+ Salt, 20 mM HEPES, 100 mM KCl, 100 mM NMDG-Cl. Uptake buffer contained: 20 mM HEPES, 100 mM KCl, 100 mM NaCl, 1 mM L-ascorbic acid, 1 mM EDTA. Monitoring the inward transport of Na^+, two populations of liposomes with two distinct intra-proteoliposomal buffers were prepared as to observe the dependence of K^+. Intra-proteoliposomal buffer *with* K^+ was composed of: 10 mM Sodium Green™, Tetra (Tetramethylammonium) Salt, 20 mM HEPES, 100 mM KCl, 100 mM NMDG-Cl. Intra-proteoliposomal buffer *without* K^+ contained: 10 mM Sodium Green™, Tetra (Tetramethylammonium) Salt, 20 mM HEPES, 200 mM NMDG-Cl. Uptake buffer was composed of: 20 mM HEPES, 200 mM NaCl, 1 mM L-ascorbic acid, 1 mM EDTA. The concentration of dopamine in the uptake buffers was 0.5 µM, while the concentration of the inhibitor nortriptyline was 500 µM. All buffers were adjusted to pH 7.5, and freshly prepared on the day of the experiment.

Tracking and co-localization software for TIRF multiplexing experiments. All individual liposomes were localized and tracked using the membrane signal from the ATTO 655 membrane dye and co-localized to

the ion indicator signal. Tracking and localization was done using in-house developed python software based on previous publications[31,32] to ensure a nanometer precise localization and co-localization whilst simultaneously correcting for any potential x, and y drift introduced by the pump. Using an adapted version of previously published software[31], the background corrected signal from both the membrane dye and ion indicator were extracted to ensure correct signal integration.

Fitting single data to single exponential decay. After signal extraction, all active traces were found by manual selection and the corresponding translocation rates determined using a maximum likelihood fitting scheme as previously described[30,32]. For K^+ experiments, the decreasing intensity traces were fitted with

$$I(t) = p * e^{(-k*t)} + y$$

Where p is the amplitude, k is the rate constant and y represents the offset from zero. For Na^+ experiments, the increasing intensity traces were fitted with

$$I(t) = p * e^{(k*t)} + y$$

Where p is the amplitude, k is the rate constant and y represents the offset from zero.

References

1 Aggarwal, S. & Mortensen, O. V. Overview of Monoamine Transporters. *Curr Protoc Pharmacol* **79**, 12.16.11-12.16.17, doi:10.1002/cpph.32 (2017).

2 Saier, M. H., Jr., Tran, C. V. & Barabote, R. D. TCDB: the Transporter Classification Database for membrane transport protein analyses and information. *Nucleic Acids Res* **34**, D181-D186 (2006).

3 Bröer, S. & Gether, U. The solute carrier 6 family of transporters. *Br J Pharmacol* **167**, 256-278, doi:10.1111/j.1476-5381.2012.01975.x (2012).

4 Rudnick, G. & Nelson, P. J. Platelet 5-hydroxytryptamine transport, an electroneutral mechanism coupled to potassium. *Biochemistry* **17**, 4739-4742, doi:10.1021/bi00615a021 (1978).

5 Wise, R. A. Dopamine, learning and motivation. *Nat Rev Neurosci* **5**, 483-494, doi:10.1038/nrn1406 (2004).

6 Sotnikova, T. D., Beaulieu, J. M., Gainetdinov, R. R. & Caron, M. G. Molecular biology, pharmacology and functional role of the plasma membrane dopamine transporter. *CNS. Neurol. Disord. Drug Targets* **5**, 45-56 (2006).

7 Hansen, F. H. *et al.* Missense dopamine transporter mutations associate with adult parkinsonism and ADHD. *J Clin Invest* **124**, 3107-3120, doi:10.1172/JCI73778 (2014).

8 Cook, E. H., Jr. *et al.* Association of attention-deficit disorder and the dopamine transporter gene. *Am J Hum Genet* **56**, 993-998 (1995).

9 Beuming, T. *et al.* The binding sites for cocaine and dopamine in the dopamine transporter overlap. *Nat Neurosci* **11**, 780-789, doi:10.1038/nn.2146 (2008).

10 Giros, B., Jaber, M., Jones, S. R., Wightman, R. M. & Caron, M. G. Hyperlocomotion and indifference to cocaine and amphetamine in mice lacking the dopamine transporter. *Nature* **379**, 606-612 (1996).

11 Chen, R. *et al.* Abolished cocaine reward in mice with a cocaine-insensitive dopamine transporter. *Proc. Natl. Acad. Sci. U. S. A* **103**, 9333-9338 (2006).

12 Robertson, S. D., Matthies, H. J. G. & Galli, A. A closer look at amphetamine-induced reverse transport and trafficking of the dopamine and norepinephrine transporters. *Mol Neurobiol* **39**, 73-80, doi:10.1007/s12035-009-8053-4 (2009).

13 Yamashita, A., Singh, S. K., Kawate, T., Jin, Y. & Gouaux, E. Crystal structure of a bacterial homologue of Na+/Cl–dependent neurotransmitter transporters. *Nature* **437**, 215-223 (2005).

14 Forrest, L. R. & Rudnick, G. The rocking bundle: a mechanism for ion-coupled solute flux by symmetrical transporters. *Physiology. (Bethesda.)* **24**, 377-386, doi:24/6/377 [pii];10.1152/physiol.00030.2009 [doi] (2009).

15 Keyes, S. R. & Rudnick, G. Coupling of transmembrane proton gradients to platelet serotonin transport. *J Biol Chem* **257**, 1172-1176 (1982).

16 Billesbølle, C. B. *et al.* Transition metal ion FRET uncovers K+ regulation of a neurotransmitter/sodium symporter. *Nature Communications* **7**, 12755, doi:10.1038/ncomms12755 (2016).

17 Merkle, P. S. *et al.* Substrate-modulated unwinding of transmembrane helices in the NSS transporter LeuT. *Sci Adv* **4**, eaar6179, doi:10.1126/sciadv.aar6179 (2018).

18 Khelashvili, G. *et al.* Conformational Dynamics on the Extracellular Side of LeuT Controlled by Na+ and K+ Ions and the Protonation State of Glu290. *J Biol Chem* **291**, 19786-19799, doi:10.1074/jbc.M116.731455 (2016).

19 Zhang, Y. W. *et al.* Structural elements required for coupling ion and substrate transport in the neurotransmitter transporter homolog LeuT. *Proc Natl Acad Sci U S A* **115**, E8854-e8862, doi:10.1073/pnas.1716870115 (2018).

20 Nielsen, A. K. *et al.* Substrate-induced conformational dynamics of the dopamine transporter. *Nat Commun* **10**, 2714, doi:10.1038/s41467-019-10449-w (2019).

21 Penmatsa, A., Wang, K. H. & Gouaux, E. X-ray structure of dopamine transporter elucidates antidepressant mechanism. *Nature* **503**, 85-90, doi:nature12533 [pii];10.1038/nature12533 [doi] (2013).

22 Pörzgen, P., Park, S. K., Hirsh, J., Sonders, M. S. & Amara, S. G. The antidepressant-sensitive dopamine transporter in Drosophila melanogaster: a primordial carrier for catecholamines. *Mol Pharmacol* **59**, 83-95, doi:10.1124/mol.59.1.83 (2001).

23 Humphreys, C. J., Beidler, D. & Rudnick, G. Substrate and inhibitor binding and translocation by the platelet plasma membrane serotonin transporter. *Biochem Soc Trans* **19**, 95-98, doi:10.1042/bst0190095 (1991).

24 Dukkipati, A., Park, H. H., Waghray, D., Fischer, S. & Garcia, K. C. BacMam system for high-level expression of recombinant soluble and membrane glycoproteins for structural studies. *Protein Expr. Purif* **62**, 160-170, doi:S1046-5928(08)00213-1 [pii];10.1016/j.pep.2008.08.004 [doi] (2008).

25 Goehring, A. *et al.* Screening and large-scale expression of membrane proteins in mammalian cells for structural studies. *Nat. Protocols* **9**, 2574-2585 (2014).

26 Wyllie, D. J. & Chen, P. E. Taking the time to study competitive antagonism. *Br J Pharmacol* **150**, 541-551, doi:10.1038/sj.bjp.0706997 (2007).

27 Newman, A. H., Zou, M. F., Ferrer, J. V. & Javitch, J. A. [3H]MFZ 2-12: a novel radioligand for the dopamine transporter. *Bioorg Med Chem Lett* **11**, 1659-1661, doi:10.1016/s0960-894x(01)00271-2 (2001).

28 Skinner, J. J., Lim, W. K., Bédard, S., Black, B. E. & Englander, S. W. Protein dynamics viewed by hydrogen exchange. *Protein Sci* **21**, 996-1005, doi:10.1002/pro.2081 (2012).

29 Wang, K. H., Penmatsa, A. & Gouaux, E. Neurotransmitter and psychostimulant recognition by the dopamine transporter. *Nature* **521**, 322-327, doi:10.1038/nature14431 (2015).

30 Thomsen, R. P. *et al.* A large size-selective DNA nanopore with sensing applications. *Nat Commun* **10**, 5655, doi:10.1038/s41467-019-13284-1 (2019).

31 Bohr, S. S., Thorlaksen, C., Kuhnel, R. M., Gunther-Pomorski, T. & Hatzakis, N. S. Label-Free Fluorescence Quantification of Hydrolytic Enzyme Activity on Native Substrates Reveals How Lipase

Function Depends on Membrane Curvature. *Langmuir* **36**, 6473-6481, doi:10.1021/acs.langmuir.0c00787 (2020).

32 Hatzakis, N. S. *et al.* How curved membranes recruit amphipathic helices and protein anchoring motifs. *Nat Chem Biol* **5**, 835-841, doi:10.1038/nchembio.213 (2009).

33 Möller, I. R. *et al.* Conformational dynamics of the human serotonin transporter during substrate and drug binding. *Nat Commun* **10**, 1687, doi:10.1038/s41467-019-09675-z (2019).

34 Mager, S. *et al.* Conducting states of a mammalian serotonin transporter. *Neuron* **12**, 845-859 (1994).

35 Sonders, M. S., Zhu, S. J., Zahniser, N. R., Kavanaugh, M. P. & Amara, S. G. Multiple ionic conductances of the human dopamine transporter: the actions of dopamine and psychostimulants. *J Neurosci* **17**, 960-974 (1997).

36 Herborg, F., Andreassen, T. F., Berlin, F., Loland, C. J. & Gether, U. Neuropsychiatric disease-associated genetic variants of the dopamine transporter display heterogeneous molecular phenotypes. *Journal of Biological Chemistry* **293**, 7250-7262, doi:10.1074/jbc.RA118.001753 (2018).

37 Masson, G. R. *et al.* Recommendations for performing, interpreting and reporting hydrogen deuterium exchange mass spectrometry (HDX-MS) experiments. *Nat Methods* **16**, 595-602, doi:10.1038/s41592-019-0459-y (2019).

Figures

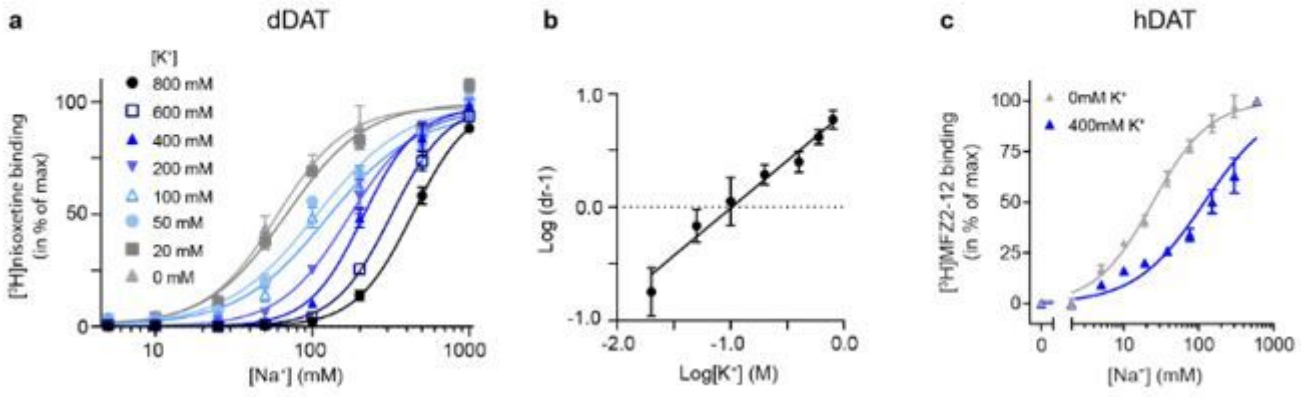

Figure 1

Na+-dependent ligand binding to DAT is inhibited by K+. (a) Na+-dependent [3H]nisoxetine binding to dDAT in mixed micelles in increasing K+ concentrations, n = 3. Lines are fit to dose-response functions

(Extended Data Table 1) (b) Schild plot from EC50 values in (a). The slope of the line = 0.84 [0.75, 0.93], K+ binding constant (KB) = 102 [100;105] mM (mean [SEM interval]). (c) Na+-dependent binding of cocaine analogue [3H]MFZ 2-12 to hDAT in membranes. Addition of 400 mM K+ increased the EC50 value from 24 [23;26] to 121 [106;134] mM (mean [SEM interval]), n = 3. In (a) and (c) data points represent means ± SEM (error bars).

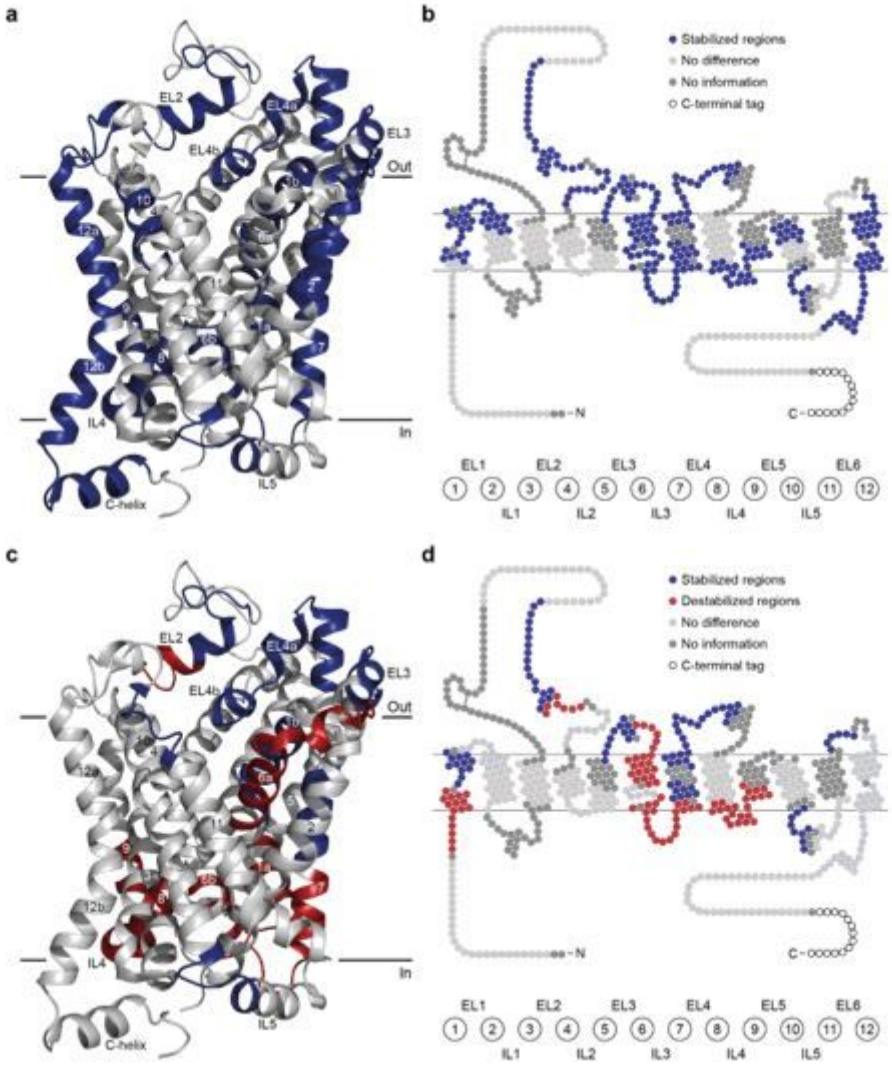

Figure 2

K+ Impacts the conformational dynamics of dDAT. (a), (b) Regions of dDAT exhibiting significant differences in deuterium uptake between the apo (Cs+) and the K+ states. The presence of K+ decreased HDX in several regions of dDAT (blue). (c), (d) Regions of dDAT exhibiting significant differences in HDX between Na+ and the K+ states. The presence of K+ induced both stabilizing (reduced HDX, blue) and destabilizing (increased HDX, red) effects in several regions of dDAT relative to the Na+-bound state. The changes in HDX are mapped onto the crystal structure (a), (c) (PDB ID: 4XP1) and a snake diagram (b), (d) of dDAT. Unchanged and uncovered regions are colored light and dark grey, respectively.

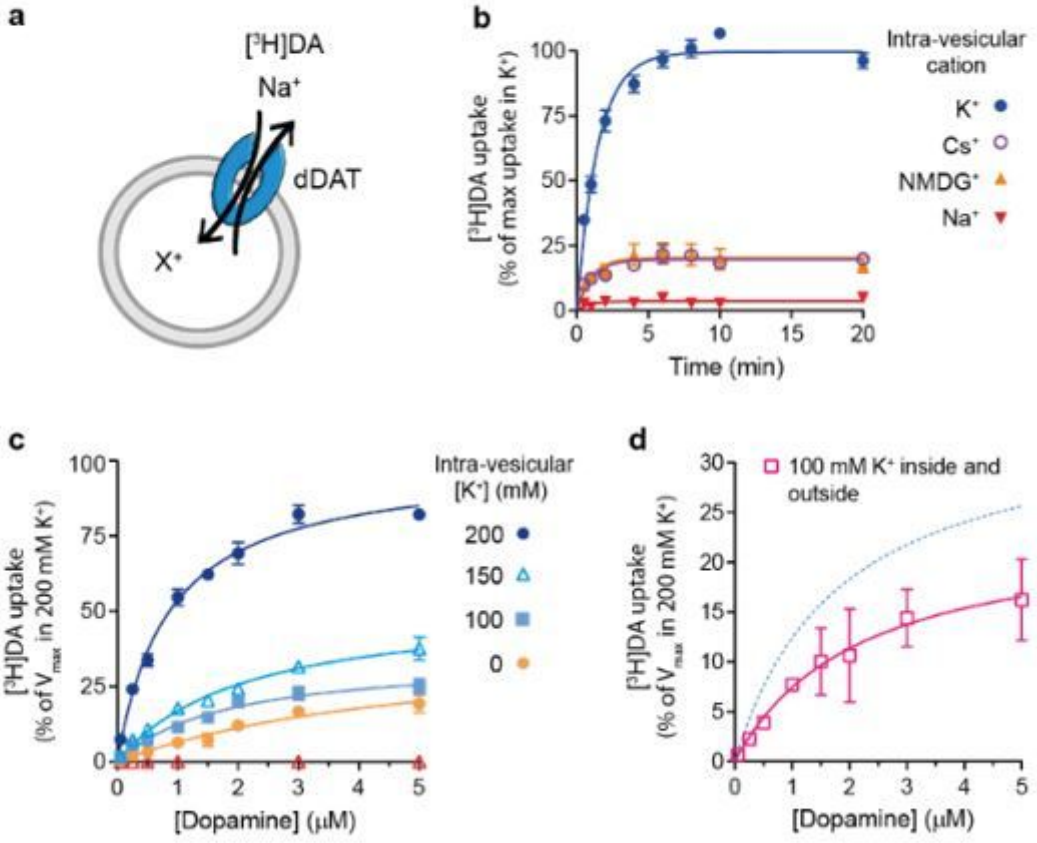

Figure 3

dDAT dopamine transport into proteoliposomes is increased by K+. (a) Schematic of PL reconstituted with varying cations in the intra-vesicular buffer (X+). (b) Time-dependent [3H]dopamine uptake. Substitution of intra-vesicular K+ with NMDG+ or Cs+ decreased the transport capacity (Extended Data Table 4), n = 3 - 4. (c) [3H]dopamine saturation uptake into PLs with varying intra-vesicular K+ concentration. Lines are fit to Michaelis-Menten kinetics (Extended Data Table 5), n = 3. (d) With equal concentrations of K+ (100 mM) on both sides uptake decreased relative to the condition with an outward directed K+ gradient (100 mM from (c), dashed line), n = 3. Statistical analysis was performed on the error-propagated Vmax estimates with a two-sided unpaired t-test, p = 0.0164. Data points in (b, c, d) represent mean ± SEM (error bars).

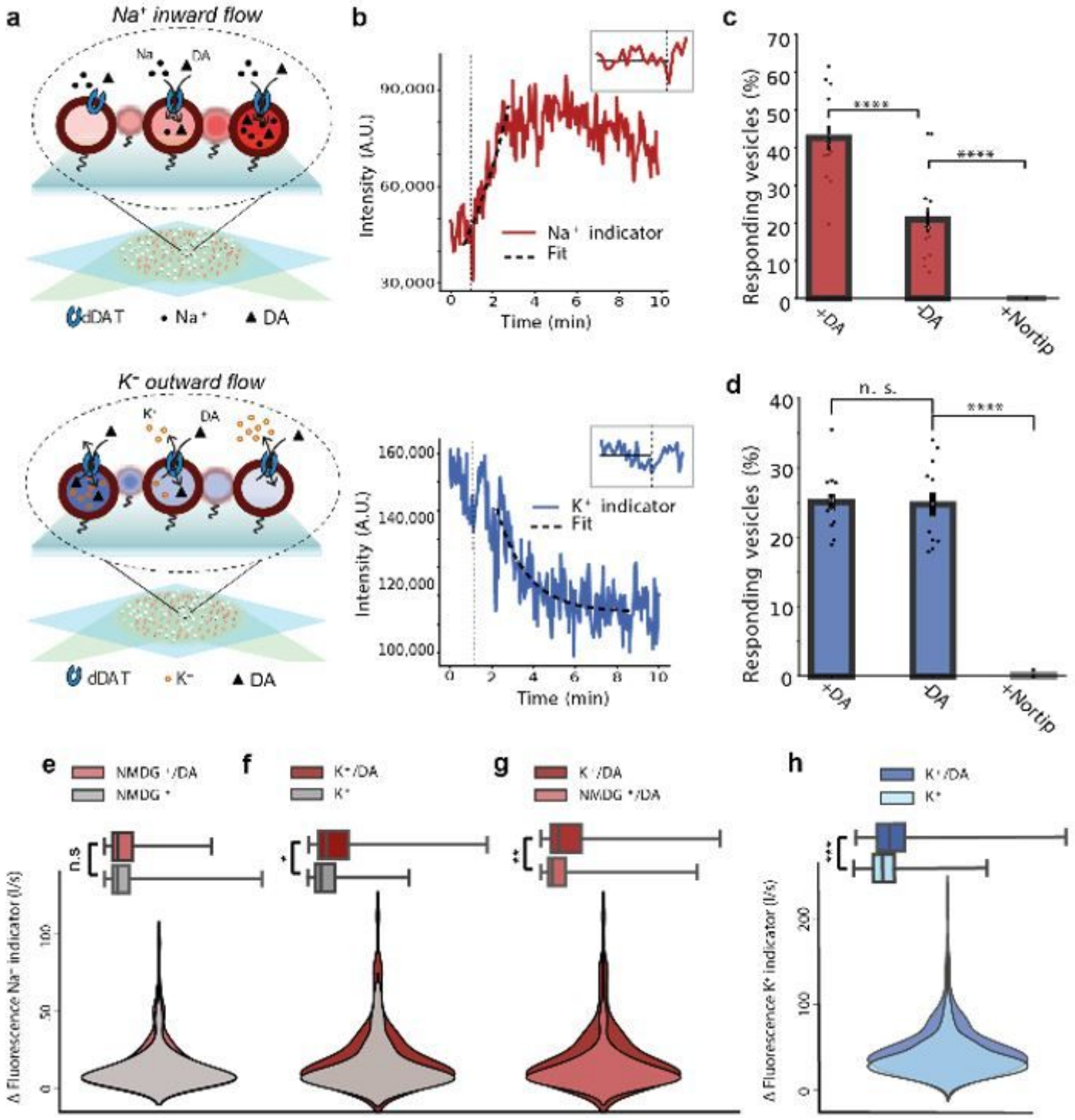

Figure 4

Time-resolved Na+ and K+ flux from single dDAT proteoliposomes. (a) Representation of single liposome measurements with TIRFm of PLs containing Na+ indicator (top) or K+ indicator (bottom). (b) Representative intensity trace from the Na+-indicator (top) or K+-indicator (bottom) from a single vesicle after addition (inset and dashed line) of uptake buffer. (c) The percentage of vesicles showing fluorescence increase in the Na+ indicator signal after addition of uptake buffer without dopamine (-DA)

20.8 ± 3.3 % and with dopamine (+DA) 42.5 ± 3.3 %. Addition of nortriptyline (+Nortrip) to the uptake buffer inhibited the response. Data points represent the percentage of responding PLs from a surface (approximately 300 PLs), bar plot represents the mean ± SEM, (n = 12). (d) As in (c) but shown for vesicles containing the K+ indicator responding with a decay in fluorescence. Responding vesicles was 25.0 ± 4.3 % with dopamine and 24.7 ± 5.7 % without. No responses were observed when nortriptyline (+Nortrip) was added. Bar plot represents mean ± SEM, (n = 12). Significance was determined by a two-sided KS test and a two-sided t-test: n.s. indicates $p > 0.05$, **** indicates $p < 0.0001$. (e, f, g) Bottom panels: Violin plots displaying the probability distribution of the rates of fluorescence change from the Na+ indicator from single PLs containing either NMDG+ or K+, measured with and without DA in the uptake buffer. The width of the plots display the kernel density of the rates. Top panels: Box plots showing the median and statistical dispersion of the fluorescence increase rates from the violin plots. The statistical significance of the difference between the distributions was evaluated with a two-sided KS-test. For the violin plots (e) not significant, $p = 0.74$, (f) $p = 0.044$, (g) $p < 0.007$ (h) Violin and bar plots of the rates of signal decrease obtained from the K+ indicator. Two sided KS-test for violin plots, $p < 0.001$.

Supplementary Files

This is a list of supplementary files associated with this preprint. Click to download.

- SchmidtetalKaffectsdDATactivityExtdData.docx